This is the accepted manuscript made available via CHORUS. The article has been published as:

Bump in the blue axion isocurvature spectrum

Daniel J. H. Chung and Amol Upadhye

Phys. Rev. D **95**, 023503 — Published 6 January 2017

DOI: 10.1103/PhysRevD.95.023503

A Bump in the Blue Axion Isocurvature Spectrum

Daniel J. H. Chung* and Amol Upadhye†
Department of Physics, University of Wisconsin-Madison, Madison, WI 53706, USA

Blue axion isocurvature perturbations are both theoretically well-motivated and interesting from a detectability perspective. These power spectra generically have a break from the blue region to a flat region. Previous investigations of the power spectra were analytic, which left a gap in the predicted spectrum in the break region due to the non-applicability of the used analytic techniques. We therefore compute the isocurvature spectrum numerically for an explicit supersymmetric axion model. We find a bump that enhances the isocurvature signal for this class of scenarios. A fitting function of three parameters is constructed that fits the spectrum well for the particular axion model we study. This fitting function should be useful for blue isocurvature signal hunting in data and making experimental sensitivity forecasts.

1. INTRODUCTION

In many proposals beyond the standard model (SM) of particle physics, massive fields that live long enough to be dark matter candidates commonly exist and could have been dynamical during inflation. The well-known η-problem in inflation [1] is a statement of genericity of massive scalar fields with temporary masses of order H (expansion rate) during inflation for models involving gravity (such as supergravity) [2–4]. Some of these fields generically do not carry large energy density during inflation (i.e. they are not in the inflaton sector and are often called spectators), and they will have de Sitter temperature induced inhomogeneities which have a blue power spectrum due to the field masses of order H (see for example [5]). If these fields are sufficiently secluded from both the inflaton sector and the SM sector (*i.e.* they are only very weakly interacting), the blue spectrum will survive long enough for them to be observable today [6] in the form of isocurvature perturbations [7–10].[1] However, if the masses of order H do not undergo a transition to a different value at some point *during* inflation, the energy density dilution during inflation can make these noninflaton fields' isocurvature perturbations nearly impossible to observe directly even if they had a large amplitude blue isocurvature spectrum [15]. Furthermore, a good theoretical motivation for such a dark matter candidate is often desirable.

Axions [16–23], which are well motivated from the perspective of solving the strong CP problem, therefore are good candidates for generating blue isocurvature perturbations [24]. The current phenomenological bounds require the axions to be very weakly interacting [23, 25–27], and therefore there is a phenomenological motivation for their seclusion from the SM sector beyond the considerations of isocurvature perturbations. Because they are pseudo-Nambu-Goldstone bosons, their coupling to the inflaton can also naturally be limited, and therefore, one can easily motivate their seclusion from the inflaton sector. Next comes a most interesting ingredient. Even though axion masses are protected by an anomalous global $U(1)_{PQ}$ (i.e. Peccei-Quinn symmetry denoted as PQ symmetry), they would generically acquire masses of the order of PQ order parameter field mass during inflation if the PQ order parameter field is out of equilibrium and moving to its potential minimum [28]. Through the η-problem mechanism discussed above, PQ order parameter field can naturally have a mass of order H, and therefore the axion temporarily has a mass of order H until the PQ order parameter reaches its minimum. Consequently, the axion mass generically shuts off at some point during inflation, allowing their energy density to survive inflationary dilution. During the time when the axion mass has not shut off, axion quantum fluctuations generate blue spectral inhomogeneities. Hence, axions possess all the necessary ingredients for naturally generating an observable blue isocurvature spectrum.

Blue axion isocurvature perturbations are therefore both theoretically and observationally well-motivated. Previous investigations of the power spectra were analytic [24, 28], leaving a gap in the predicted primordial power spectrum near the spectral scale where the axion mass turns off. In this work, we numerically investigate this analytic gap region and find that there is a bump in the power spectrum. This bump enhances the isocurvature amplitude by an order unity factor, and such enhancements can facilitate the observational detection or exclusion of this class of models. We construct an economical fitting function Eq. (119) consisting of only 3 parameters. The fitting function will be useful in hunting for such blue spectral signals in current and future observational data. We also verify that the change in the isocurvature amplitude after the end of inflation is of the expected negligible magnitude of $(H/F_a)^2 \ll 1$.

The order of presentation will be as follows, in the next section we review the axion model of [24] that we wish to study in detail. In Sec. 3, we explain how the numerical problem will be set up to deal with the issue of Planck scale oscillation modes

*Electronic address: danielchung@wisc.edu
†Electronic address: aupadhye@wisc.edu

[1] Non-Gaussianities discussed for example in [11–14] do not necessarily require such weak interactions.

becoming light. In Sec. 4, we present the numerical computational results including the fitting function. We conclude with a summary of the work.

2. AXION MODEL

For concreteness of our numerical investigation, we consider the model of [24]. The qualitative features of this model are expected to be generic, although quantitatively, the details may differ.

The authors of [24] consider a supersymmetric axion model with the following renormalizable superpotential

$$W = h(\Phi_+\Phi_- - F_a^2)\Phi_0 \tag{1}$$

where the subscripts on Φ indicate $U(1)_{PQ}$ global Peccei-Quinn (PQ) charges. The F-term potential is

$$V_F = h^2|\Phi_+\Phi_- - F_a^2|^2 + h^2(|\Phi_+|^2 + |\Phi_-|^2)|\Phi_0|^2. \tag{2}$$

A flat directions of V_F exists along

$$\Phi_+\Phi_- = F_a^2 \qquad \Phi_0 = 0. \tag{3}$$

The existence of this flat direction is important because this is the reason why the effective PQ parameters will be rolling with a mass of order H during inflation (instead of being much heavier and having already settled down), taking advantage of the inflationary η-problem. Their low-scale SUSY-breaking terms are assumed to be

$$V_{\text{soft}} = m_+^2|\Phi_+|^2 + m_-^2|\Phi_-|^2 + m_0^2|\Phi_0|^2 \tag{4}$$

where $m_i = O(\text{TeV})$. For most of the inflationary dynamics, these parameters are irrelevant. The Kaehler potential induced scalar potential is

$$V_K = c_+H^2|\Phi_+|^2 + c_-H^2|\Phi_-|^2 + c_0H^2|\Phi_0|^2 \tag{5}$$

where $c_{+,-,0}$ are positive $O(1)$ constants. The parameter c_+ dominantly controls the blue spectral index. This setup implicitly assumes that the inflaton sector can be arranged to have $H \ll F_a$ such that the flat directions are only lifted by the quadratic terms at the renormalizable level.

Looking along the flat direction of Eq. (3), we set $\Phi_0 = 0$. The resulting relevant effective potential during inflation is

$$V \approx h^2|\Phi_+\Phi_- - F_a^2|^2 + c_+H^2|\Phi_+|^2 + c_-H^2|\Phi_-|^2. \tag{6}$$

During inflation, the minimum of $\Phi_\pm$ lies at

$$|\Phi_\pm^{\text{min}}| \approx \left(\frac{c_\mp}{c_\pm}\right)^{1/4} F_a. \tag{7}$$

The key initial condition is that $\Phi_\pm$ starts out away from the minimum with a magnitude much larger than $O(F_a)$ and rolls towards the minimum during inflation. This implies the $U(1)_{PQ}$ symmetry is broken during inflation. Hence, there will be a linear combination of the phases of $\Phi_\pm$ which will be the Nambu-Goldstone boson associated with the broken $U(1)_{PQ}$. In particular, with the parameterization

$$\Phi_\pm \equiv \frac{\varphi_\pm}{\sqrt{2}} \exp\left(i\frac{a_\pm}{\sqrt{2}\varphi_\pm}\right) \tag{8}$$

where $\varphi_\pm$ and $a_\pm$ are real, the axion is

$$a = \frac{\varphi_+}{\sqrt{\varphi_+^2 + \varphi_-^2}} a_+ - \frac{\varphi_-}{\sqrt{\varphi_+^2 + \varphi_-^2}} a_- \tag{9}$$

while the heavier combination

$$b = \frac{\varphi_-}{\sqrt{\varphi_+^2 + \varphi_-^2}} a_+ + \frac{\varphi_+}{\sqrt{\varphi_+^2 + \varphi_-^2}} a_- \tag{10}$$

is governed by the potential

$$V_b = -h^2 F_a^2 \varphi_+ \varphi_- \cos\left(\frac{\sqrt{\varphi_+^2+\varphi_-^2}}{\varphi_+\varphi_-} b\right). \tag{11}$$

Since the b field is heavy (*i.e.* $(\varphi_+^2+\varphi_-^2)F_a^2/(\varphi_+\varphi_-) \gg H^2$), it is not dynamically important. Hence, one can gain some intuition for how the axion composition time evolves by setting $b=0$. When φ_+ is large, the axion is dominantly a_+ and later when φ_+ becomes comparable to φ_-, the axion is a mixture of a_- and a_+.

3. SETUP OF THE NUMERICAL PROBLEM

Here we present a semi-numerical approach to the mode problem. In setting up the numerical problem, the equation of motion in terms of a field is far more complicated than in the $\{\Phi_\pm, \Phi_0\}$ basis. We will therefore set up the spectral numerical computation in terms of $\{\Phi_\pm, \Phi_0\}$. The background equations are

$$\ddot{\Phi}_+ + 3H\dot{\Phi}_+ + (c_+H^2+m_+^2)\Phi_+ + h^2(\Phi_+\Phi_- - F_a^2)\Phi_-^* + h^2\Phi_+|\Phi_0|^2 = 0 \tag{12}$$

$$\ddot{\Phi}_- + 3H\dot{\Phi}_- + (c_-H^2+m_-^2)\Phi_- + h^2(\Phi_+\Phi_- - F_a^2)\Phi_+^* + h^2\Phi_-|\Phi_0|^2 = 0 \tag{13}$$

$$\ddot{\Phi}_0 + 3H\dot{\Phi}_0 + (c_0H^2+m_0^2)\Phi_0 + h^2(|\Phi_+|^2+|\Phi_-|^2)\Phi_0 = 0 \tag{14}$$

and the fluctuation equations in Fourier space are

$$\begin{aligned}\delta\ddot{\Phi}_+ + 3H\delta\dot{\Phi}_+ + (c_+H^2+m_+^2+\frac{k^2}{a^2})\delta\Phi_+ + h^2(\Phi_+\Phi_- - F_a^2)\delta\Phi_-^* + h^2\delta\Phi_+|\Phi_0|^2 \\ +h^2(\Phi_+\delta\Phi_-)\Phi_-^* + h^2(\delta\Phi_+\Phi_-)\Phi_-^* + h^2\Phi_+\delta\Phi_0\Phi_0^* + h^2\Phi_+\Phi_0\delta\Phi_0^* \;=\; 0\end{aligned} \tag{15}$$

$$\begin{aligned}\delta\ddot{\Phi}_- + 3H\delta\dot{\Phi}_- + (c_-H^2+m_-^2+\frac{k^2}{a^2})\delta\Phi_- + h^2(\Phi_+\Phi_- - F_a^2)\delta\Phi_+^* + h^2\delta\Phi_-|\Phi_0|^2 \\ +h^2(\delta\Phi_+\Phi_-)\Phi_+^* + h^2(\Phi_+\delta\Phi_-)\Phi_+^* + h^2\Phi_-\delta\Phi_0\Phi_0^* + h^2\Phi_-\Phi_0\delta\Phi_0^* \;=\; 0\end{aligned} \tag{16}$$

$$\begin{aligned}\delta\ddot{\Phi}_0 + 3H\delta\dot{\Phi}_0 + (c_0H^2+m_0^2+\frac{k^2}{a^2})\delta\Phi_0 + h^2(|\Phi_+|^2+|\Phi_-|^2)\delta\Phi_0 \\ +h^2(\Phi_+\delta\Phi_+^* + \delta\Phi_+\Phi_+^* + \delta\Phi_-\Phi_-^* + \Phi_-\delta\Phi_-^*)\Phi_0 \;=\; 0.\end{aligned} \tag{17}$$

Since we are interested in flat direction solutions to the background equations and since the Φ_0 mass is extremely large for the large displacements of Φ_+ that we are interested in, we restrict ourselves to the

$$\Phi_0 = 0 \tag{18}$$

solution to the equations of motion. This simplifies the perturbation equations significantly. Furthermore, we can rephase the the background fields such that only real background functions need to be evolved because of the CP symmetry of the background equations. This means that if we set the initial condition such that

$$\tilde{\Phi}_\pm = \Phi_\pm \exp\left(\mp i\theta_+(t_\mathrm{i})\right) \tag{19}$$

where $\tilde{\Phi}_\pm$ is real, $\tilde{\Phi}_\pm$ will remain real. Note that the opposite rephasing of $\Phi_\pm$ initial conditions is consistent with the heavy mode $b=0$ in the background equation (see Eq. (11)). The initial time t_i must be chosen such that the longest observable wave vector k_min must be be subhorizon at time t_i.

For quantization of the fluctuations, it is also convenient to decompose the perturbations into real scalar fields $\{R_\pm, I_\pm\}$:

$$\delta\Phi_\pm = R_\pm + iI_\pm \tag{20}$$

$$\delta\Phi_0 = Z_r + iZ_i. \tag{21}$$

The quantum mode equations[2] therefore are

$$\begin{aligned}\ddot{R}_+ + 3H\dot{R}_+ + (c_+H^2 + m_+^2 + \frac{k^2}{a^2})R_+ + h^2(\tilde{\Phi}_+\tilde{\Phi}_- - F_a^2)R_- \\ +h^2[\cos(2\theta_+(t_i))R_- - \sin(2\theta_+(t_i))I_-]\tilde{\Phi}_+\tilde{\Phi}_- + h^2\tilde{\Phi}_-^2 R_+ &= 0\end{aligned} \tag{24}$$

$$\begin{aligned}\ddot{I}_+ + 3H\dot{I}_+ + (c_+H^2 + m_+^2 + \frac{k^2}{a^2})I_+ - h^2(\tilde{\Phi}_+\tilde{\Phi}_- - F_a^2)I_- \\ +h^2[\cos(2\theta_+(t_i))I_- + \sin(2\theta_+(t_i))R_-]\tilde{\Phi}_+\tilde{\Phi}_- + h^2\tilde{\Phi}_-^2 I_+ &= 0\end{aligned} \tag{25}$$

$$\begin{aligned}\ddot{R}_- + 3H\dot{R}_- + (c_-H^2 + m_-^2 + \frac{k^2}{a^2})R_- + h^2(\tilde{\Phi}_+\tilde{\Phi}_- - F_a^2)R_+ \\ +h^2(\cos(2\theta_+(t_i))R_+ + \sin(2\theta_+(t_i))I_+)\tilde{\Phi}_+\tilde{\Phi}_- + h^2\tilde{\Phi}_+^2 R_- &= 0\end{aligned} \tag{26}$$

$$\begin{aligned}\ddot{I}_- + 3H\dot{I}_- + (c_-H^2 + m_-^2 + \frac{k^2}{a^2})I_- - h^2(\tilde{\Phi}_+\tilde{\Phi}_- - F_a^2)I_+ \\ +h^2(\cos(2\theta_+(t_i))I_+ - \sin(2\theta_+(t_i))R_+)\tilde{\Phi}_+\tilde{\Phi}_- + h^2\tilde{\Phi}_+^2 I_- &= 0\end{aligned} \tag{27}$$

$$\ddot{Z}_{r,i} + 3H\dot{Z}_{r,i} + (c_0H^2 + m_0^2 + \frac{k^2}{a^2} + h^2[|\tilde{\Phi}_+|^2 + |\tilde{\Phi}_-|^2])Z_{r,i} = 0. \tag{28}$$

Note that $Z_{r,i}$ modes are completely decoupled from the other modes.

For $\theta_+(t_i) \ll 1$, the axion correlator that we are interested in computing is

$$\begin{aligned}\left\langle \frac{\delta a}{a}\frac{\delta a}{a}\right\rangle \mathscr{D} &= \langle I_-I_-\rangle\tilde{\Phi}_-^2 + \langle I_+I_+\rangle\tilde{\Phi}_+^2 - [\langle I_+I_-\rangle + \langle I_-I_+\rangle]\tilde{\Phi}_-\tilde{\Phi}_+ - [\langle I_-R_-\rangle + \langle R_-I_-\rangle]\tilde{\Phi}_-^2\theta_+(t_i) \\ &\quad - [\langle I_-R_+\rangle + \langle R_+I_-\rangle]\tilde{\Phi}_-\tilde{\Phi}_+\theta_+(t_i) + [\langle I_+R_-\rangle + \langle R_-I_+\rangle]\tilde{\Phi}_-\tilde{\Phi}_+\theta_+(t_i) \\ &\quad + [\langle I_+R_+\rangle + \langle R_+I_+\rangle]\tilde{\Phi}_+^2\theta_+(t_i)\end{aligned} \tag{29}$$

where

$$\mathscr{D} \equiv \left(\tilde{\Phi}_+^2 + \tilde{\Phi}_-^2\right)^2\theta_+^2(t_i), \tag{30}$$

and here we follow the typical abuse of notation in which the quantum fields and their mode functions are denoted with the same symbols. This correlator is related to the primordial isocurvature spectrum through the equation

$$\Delta_S^2(t,\vec{p}) = 4\omega_a^2\frac{p^3}{2\pi^2}\int\frac{d^3q}{(2\pi)^3}\left\langle\frac{\delta a(t,\vec{p})}{a}\frac{\delta a(t,\vec{q})}{a}\right\rangle \tag{31}$$

where we use the ratio of a common formula for a QCD axion energy density to cold dark matter energy density (e.g. equation 14 of [29])

$$\omega_a \equiv \frac{\Omega_a}{\Omega_{\rm cdm}} \tag{32}$$

$$= W_a\theta_+^2(t_i)\left(\frac{\sqrt{2}\left(\tilde{\Phi}_+^2(t_f) + \tilde{\Phi}_-^2(t_f)\right)^{1/2}}{10^{12}\text{GeV}}\right)^{n_{PT}} \tag{33}$$

---

[2] For example, we can write

$$\Re(\Phi_+(t,\vec{x})) = \tilde{\Phi}_+(t)\cos(\theta_+(t_i)) + \int\frac{d^3k}{(2\pi)^{3/2}}\left[a_{\vec{k}}^{(R+)}R_+e^{i\vec{k}\cdot\vec{x}} + a_{\vec{k}}^{(R+)\dagger}R_+^*e^{-i\vec{k}\cdot\vec{x}}\right] \tag{22}$$

$$\Im(\Phi_+(t,\vec{x})) = \tilde{\Phi}_+(t)\sin(\theta_+(t_i)) + \int\frac{d^3k}{(2\pi)^{3/2}}\left[a_{\vec{k}}^{(I+)}I_+e^{i\vec{k}\cdot\vec{x}} + a_{\vec{k}}^{(I+)\dagger}I_+^*e^{-i\vec{k}\cdot\vec{x}}\right] \tag{23}$$

in a creation-annihilation operator expansion where $\{R_+, I_+\}$ are mode functions satisfying mode equations.

where $W_a \approx 1.5$ and $n_{PT} \approx 1.19$ and t_f is the time just before the QCD phase transition.[3] This formula differs from equation 203 of [28] by a factor of $2^{n_{PT}/2}$ because of a mistake in the way the axion decay constant was defined there. Here we are defining the effective decay constant as

$$f_a = \sqrt{2}\left(\tilde{\Phi}_+^2(t_f) + \tilde{\Phi}_-^2(t_f)\right)^{1/2}. \tag{34}$$

Each of the correlators in Eq. (29) is computed using the procedure as specified in [29]. For example, the I_+ correlator is computed as

$$\langle I_+ I_+ \rangle \to \langle I_+(t,\vec{p}) I_+(t,\vec{q}) \rangle = (2\pi)^3 \sum_{\alpha=1}^{4} I_+^{(\alpha)}(t,\vec{p}) I_+^{(\alpha)*}(t,\vec{q}) \delta^{(3)}(\vec{q}+\vec{p}) \tag{35}$$

where the α-labeled boundary conditions will be discussed shortly (around Eq. (36)). The goal of the rest of this section is to set up the numerical problem to compute $\Delta_S^2(t,\vec{p})/\omega_a^2$ to about 20% accuracy after the end of inflation for a wide range of parameters which are $\{c_+,\ c_-,\ F_a,\ H,\ \tilde{\Phi}_+(t_i),\ \theta(t_i),\ h\}$ where t_i is the initial time during inflation when the effective field theory describing this axion model is valid.[4] Although the accuracy goal may naively seem poor, it is actually only modestly larger than the Planck bound since a 20% accuracy and an isocurvature fraction of about 10% implies a few percent accuracy in the total power spectrum. Note $m_\pm \ll H$ is assumed such that they are not relevant for this computation. Also, note that we do not need to compute $Z_{r,i}$ since they do not mix with $\{R_\pm, I_\pm\}$ and do not enter in Eq. (29). We will henceforth drop any discussion of $Z_{r,i}$.

3.1. Ideal initial conditions

As noted in [30], to stay consistent with the tree-level truncation of the in-in formalism, we should set one of $\psi \equiv (R_+, I_+, R_-, I_-)$ modes initially non-zero and every other mode initially zero. The non-zero boundary condition should be adiabatic (which is approximately equivalent to Bunch-Davies vacuum). For example, the boundary conditions at a time when $k \gg a(t_{i\,\mathrm{num}})H$ can be taken to be (for the numerical run α)

$$\psi_l^{(\alpha)}|_{t=t_{i\,\mathrm{num}}(k)} = (U^\dagger)_{l\alpha} \frac{N_\alpha}{\sqrt{2}\lambda_\alpha^{1/4} a^{3/2}(t_{i\,\mathrm{num}}(k))} \tag{36}$$

$$\frac{d}{dt}\psi_l^{(\alpha)}|_{t=t_{i\,\mathrm{num}}(k)} = -i(U^\dagger)_{l\alpha} \frac{N_\alpha \lambda_\alpha^{1/4}}{\sqrt{2} a^{3/2}(t_{i\,\mathrm{num}}(k))} \tag{37}$$

where

$$N_\alpha = \frac{1}{\sqrt{2}} \tag{38}$$

is a normalization factor that can come from non-canonical normalization of the kinetic term, U is a mixing matrix that diagonalizes the dispersion squared matrix, and we are assuming that the mixing matrix time derivative is negligible at the time of the initial conditions. Note the minus sign on the "i" corresponds to defining the positive frequency modes. However, this procedure is numerically expensive and impractical since some of the eigenvalues start close to Planckian mass values and the oscillations need to be tracked until the time when the mass scales reach 10^{11} GeV.

3.2. Semi-numerical WKB approach and boundary conditions for full numerics

For long wavelength modes, $k/(aH) \gg 1$ corresponds to times when $\tilde{\Phi}_+(t) \sim O(M_p)$. This means that some of the long wavelength modes in $\psi = (R_+, I_+, R_-, I_-)$ have Planckian masses during this time and one might naively set boundary conditions for modes when the oscillation frequency is of order the Planck scale. Because Planck scale frequency oscillations are physically irrelevant for our observables, such modes can be integrated out. However, the masses eventually change as a function of time

[3] The fields $\tilde{\Phi}_\pm$ have settled down long before this.
[4] Also, for the target level of accuracy, we can ignore slow-roll evolution of the expansion rate during inflation and set H to be a constant.

such that these modes become relevant. For the numerical approach, we need a prescription to set the boundary conditions for the shorter wavelength modes whose oscillation frequency is always small consistently with the longer wavelength modes which start with Planckian oscillations and become non-Planckian. We construct below a consistent prescription that can be described as follows. For long wavelength heavy modes, we use analytic WKB solutions which are accurate. For lighter long wavelength modes, we take a semi-numerical modified WKB approach to solve the modes accurately in possible turning point regions. When the WKB and the modified WKB solutions begin to depart from being excellent approximations, all the masses are of order $F_a \ll M_p$ or smaller, and we can during this period safely compute all the modes numerically without the expense of computing irrelevant fast oscillations.

First, let us set up the math problem explicitly. As noted before, because $\delta\Phi_0$ oscillations do not contribute to the tree-level correlator we wish to compute, we can reduce the numerical problem to 4 real quantum fields containing 4 independent complex modes.[5] For the numerical study which aims for an accuracy of about 20%, we set H =constant during inflation[6] and define the ψ vector to be

$$\psi \equiv (R_+, I_+, R_-, I_-) \tag{39}$$

to write the complex mode equations as

$$\psi'' + 3\psi' + M^2\psi = 0 \tag{40}$$

where

$$M^2 \equiv \begin{pmatrix} \frac{\mu_+^2}{H^2} I & \frac{\mu_-^2}{H^2} Q^{(+)} \\ \frac{\mu_-^2}{H^2} Q^{(-)} & \frac{\mu_-^2}{H^2} I \end{pmatrix} \tag{41}$$

$$Q^{(\pm)} = \frac{h^2\tilde{\Phi}_+\tilde{\Phi}_-}{\mu_-^2}\left[I + \begin{pmatrix} \cos 2\theta - 1 & \mp\sin 2\theta \\ \pm\sin 2\theta & \cos 2\theta - 1 \end{pmatrix}\right] + \frac{h^2}{\mu_-^2}(\tilde{\Phi}_+\tilde{\Phi}_- - F_a^2)\sigma^{(3)}_{\alpha\beta} \tag{42}$$

$$\mu_\pm^2 = h^2\tilde{\Phi}_\mp^2 + c_\pm H^2 + m_\pm^2 + \frac{k^2}{a^2} \tag{43}$$

$$\sigma^{(3)} = \begin{pmatrix} 1 & 0 \\ 0 & -1 \end{pmatrix} \tag{44}$$

where $m_\pm^2$ are small quantities irrelevant for leading approximation cosmology. We want to solve this problem following the mode from the subhorizon period until past the end of inflation. During this entire period of interest, there are subhorizon WKB approximate oscillations, horizon-crossing possibly involving turning points for light modes, and a nonadiabatic period when WKB approximation breaks down and one must solve the mode equations fully numerically. The utility of the modified WKB approach below will be that it will set up a numerical problem that smoothly connects the WKB and the turning point regions into a differential equation for a single complex function (not a vector of complex functions) without necessitating the definition of an arbitrary turning point for light modes.

To diagonalize the mass squared matrix, we rewrite it as follows:

$$M^2 = M_0^2 + \lambda_{21}\Delta_{21} + \lambda_{22}\Delta_{22} + \lambda_{33}\Delta_3 \tag{45}$$

where

$$\Delta_{21} = \begin{pmatrix} 0 & I \\ I & 0 \end{pmatrix} \tag{46}$$

$$\lambda_{21} \equiv \frac{h^2(\cos 2\theta - 1)\Phi_+\Phi_-}{H^2} \tag{47}$$

---

[5] The modes $Z_{R,i}$ do not mix with the rest of the modes in Eqs. (24) through (28).

[6] Secular effects due to time evolving H give a correction of order 10ε during the $O(10)$ e-folds of inflationary phase that is observable.

$$\Delta_{22} = \begin{pmatrix} 0 & -i\sigma^{(2)}_{\alpha\beta} \\ i\sigma^{(2)}_{\alpha\beta} & 0 \end{pmatrix} \tag{48}$$

$$\lambda_{22} \equiv \frac{h^2\Phi_+\Phi_-\sin 2\theta}{H^2} \tag{49}$$

$$\Delta_3 = \begin{pmatrix} 0 & \sigma^{(3)}_{\alpha\beta} \\ \sigma^{(3)}_{\alpha\beta} & 0 \end{pmatrix} \tag{50}$$

$$\lambda_{33} \equiv \frac{h^2}{H^2}(\Phi_+\Phi_- - F_a^2) \tag{51}$$

$$\sigma^{(2)} = \begin{pmatrix} 0 & -i \\ i & 0 \end{pmatrix}. \tag{52}$$

The first eigenvalue is

$$E_1^2 = \frac{W_D^2 - \sqrt{4F_2^4 + W_-^4 - 4\lambda_{33}^2 H^4\left(\frac{2F_2^2}{\lambda_{33}H^2} - 1\right)}}{2H^2} \tag{53}$$

and the corresponding eigenvector is

$$|E_1^2\rangle = \mathcal{N}_1(a_1, b_1, c_1, 1) \qquad \mathcal{N}_1 \equiv \left(a_1^2 + b_1^2 + c_1^2 + 1\right)^{-1/2} \tag{54}$$

$$a_1 = \frac{\left(F_2^2 - \tilde{F}_a^2 h^2\right)}{2\lambda_{22}H^2}\left(\sqrt{4 + \frac{W_-^4}{\left(F_2^2 - \lambda_{33}H^2\right)^2}} + \frac{W_-^2}{F_2^2 - \lambda_{33}H^2}\right) \tag{55}$$

$$\approx \frac{\lambda_{22}H^2}{2h^2\tilde{F}_a^2}\left(\sqrt{1 + \frac{W_-^4}{4\left(F_2^2 - \lambda_{33}H^2\right)^2}} + \frac{W_-^2}{2\left(F_2^2 - \lambda_{33}H^2\right)}\right) \tag{56}$$

$$b_1 = -\sqrt{1 + \frac{W_-^4}{4\left(F_2^2 - \lambda_{33}H^2\right)^2}} - \frac{W_-^2}{2\left(F_2^2 - \lambda_{33}H^2\right)} \tag{57}$$

$$c_1 = \frac{F_2^2 - \tilde{F}_a^2 h^2}{\lambda_{22}H^2} \tag{58}$$

$$\approx \frac{\lambda_{22}H^2}{2h^2\tilde{F}_a^2} \tag{59}$$

$$F_2^4 \equiv h^4\tilde{F}_a^4 + \lambda_{22}^2 H^4 \tag{60}$$

$$W_D^2 \equiv h^2[\Phi_+^2 + \Phi_-^2] + (c_+ + c_-)H^2 + 2\frac{k^2}{a^2} \tag{61}$$

$$W_-^2 \equiv h^2(\Phi_+^2 - \Phi_-^2) + (c_- - c_+)H^2 \tag{62}$$

$$\tilde{F}_a^2 \equiv F_a^2 + \frac{\lambda_{21} H^2}{h^2} \tag{63}$$

where we will generally denote unit normalization factors as $\mathcal{N}_i$ for the ith eigenvector and we assumed

$$F_2^2 - \lambda_{33} H^2 > 0. \tag{64}$$

The next eigenvalue and eigenvector can be written similarly:

$$E_2^2 = \frac{W_D^2 + \sqrt{4F_2^4 + W_-^4 - 4\lambda_{33}^2 H^4 (\frac{2F_2^2}{\lambda_{33} H^2} - 1)}}{2H^2} \tag{65}$$

$$|E_2^2\rangle = \mathcal{N}_2 (a_2, b_2, c_2, 1) \tag{66}$$

$$a_2 = \frac{\left(F_2^2 - \tilde{F}_a^2 h^2\right)}{2\lambda_{22} H^2} \left(-\sqrt{4 + \frac{W_-^4}{\left(F_2^2 - \lambda_{33} H^2\right)^2}} + \frac{W_-^2}{F_2^2 - \lambda_{33} H^2} \right) \tag{67}$$

$$\approx \frac{\lambda_{22} H^2}{4h^2 \tilde{F}_a^2} \left(-\sqrt{4 + \frac{W_-^4}{\left(F_2^2 - \lambda_{33} H^2\right)^2}} + \frac{W_-^2}{F_2^2 - \lambda_{33} H^2} \right) \tag{68}$$

$$b_2 = \sqrt{1 + \frac{W_-^4}{4\left(F_2^2 - \lambda_{33} H^2\right)^2}} - \frac{W_-^2}{2\left(F_2^2 - \lambda_{33} H^2\right)} \tag{69}$$

$$c_2 = c_1. \tag{70}$$

The next eigenvector is interesting because one of the coefficients have a large correction with respect to the eigenvector that is obtained with $\lambda_{22} = 0$:

$$E_3^2 = \frac{W_D^2 - \sqrt{4F_2^4 + W_-^4 + 4\lambda_{33}^2 H^4 \left(\frac{2F_2^2}{\lambda_{33} H^2} + 1\right)}}{2H^2} \tag{71}$$

$$|E_3^2\rangle = \mathcal{N}_3 (a_3, b_3, c_3, \lambda_{22}) \tag{72}$$

$$a_3 = \frac{\left(F_2^2 + \tilde{F}_a^2 h^2\right)}{2H^2} \left(\sqrt{4 + \frac{W_-^4}{\left(F_2^2 + \lambda_{33} H^2\right)^2}} + \frac{W_-^2}{F_2^2 + \lambda_{33} H^2} \right) \tag{73}$$

$$b_3 = \lambda_{22} \left[\sqrt{1 + \frac{W_-^4}{4\left(F_2^2 + \lambda_{33} H^2\right)^2}} + \frac{W_-^2}{2\left(F_2^2 + \lambda_{33} H^2\right)} \right] \tag{74}$$

$$c_3 = -\frac{F_2^2 + \tilde{F}_a^2 h^2}{H^2}. \tag{75}$$

The large λ_{22} effect can be attributed to the fact that although λ_{33} is the perturbation that breaks the degeneracy, the eigenvectors with λ_{22} turned off already diagonalizes the perturbation matrix. On the other hand, when both λ_{22} and λ_{33} turn on, there is an off-diagonal matrix element of the λ_{33} perturbation in the original basis. This leads to a large degenerate perturbation theory correction. For example, b_3 is a $\lambda_{22}\lambda_{33}/\lambda_{33}$ effect. The $\lambda_{33}/\lambda_{33}$ is typical of degenerate perturbation theory effect, but λ_{22}

multiplying it shows that this is actually a second order effect in the perturbation. The fourth eigenvector system is characterized by

$$E_4^2 = \frac{W_D^2 + \sqrt{4F_2^4 + W_-^4 + 4\lambda_{33}^2 H^4 \left(\frac{2F_2^2}{\lambda_{33}H^2} + 1\right)}}{2H^2} \tag{76}$$

$$|E_4^2\rangle = \mathcal{N}_4(a_4, b_4, c_4, \lambda_{22}) \tag{77}$$

$$a_4 = \frac{\left(F_2^2 + \tilde{F}_a^2 h^2\right)}{2H^2}\left(-\sqrt{4 + \frac{W_-^4}{\left(F_2^2 + \lambda_{33}H^2\right)^2}} + \frac{W_-^2}{F_2^2 + \lambda_{33}H^2}\right) \tag{78}$$

$$b_4 = \lambda_{22}\left[-\sqrt{1 + \frac{W_-^4}{4\left(F_2^2 + \lambda_{33}H^2\right)^2}} + \frac{W_-^2}{2\left(F_2^2 + \lambda_{33}H^2\right)}\right] \tag{79}$$

$$c_4 = c_3 \tag{80}$$

We can obtain some intuition about this eigensystem if we set $\lambda_{21} = \lambda_{22} = \lambda_{33} = 0$ and keep the leading eigenvectors and their oscillation frequencies in the limit of no θ induced mixing (i.e. $\theta F_a^2/H^2 \to 0$ and $H^2/F_a^2 \to 0$) and $\{F_a^2/\Phi_+^2 \to 0,\ h^2\Phi_-^2/H^2 \to 0\}$:

$$|E_1^2 \to k^2/(aH)^2\rangle \to (0,1,0,0) \tag{81}$$

$$|E_2^2 \to h^2\Phi_+^2/H^2\rangle \to (0,0,0,1) \tag{82}$$

$$|E_3^2 \to k^2/(aH)^2\rangle \to (1,0,0,0) \tag{83}$$

$$|E_4^2 \to h^2\Phi_+^2/H^2\rangle \to (0,0,1,0) \tag{84}$$

where we have chosen the normalization factors $\mathcal{N}_i$ such that the largest component of the eigenvector is positive. The ideal initial conditions discussed abstractly in Eqs. (36) and (37) are

$$\psi^{(j)}(\eta_i)2\sqrt{E_j(\eta_i)H(\eta_i)}a^{3/2}(\eta_i) = |E_j^2(\eta_i)\rangle 2\sqrt{E_j(\eta_i)H(\eta_i)}a^{3/2}(\eta_i) \approx \mathcal{N}_j \begin{pmatrix} a_j \\ b_j \\ c_j \\ d_j \end{pmatrix} \tag{85}$$

$$\partial_\eta \psi^{(j)}(\eta_i)2\sqrt{E_j(\eta_i)H(\eta_i)}a^{3/2}(\eta_i) = -iE_j(\eta_i)|E_j^2(\eta_i)\rangle 2\sqrt{E_j(\eta_i)H(\eta_i)}a^{3/2}(\eta_i) \tag{86}$$

$$\approx -iE_j(\eta_i)\mathcal{N}_j \begin{pmatrix} a_j \\ b_j \\ c_j \\ d_j \end{pmatrix} \tag{87}$$

where

$$d_j = \begin{cases} 1 & j \in \{1,2\} \\ \lambda_{22} & j \in \{3,4\} \end{cases}. \tag{88}$$

Note the factor of $1/\sqrt{2}$ in Eq. (38) has been taken into account.

To find the WKB solution, it is convenient to eliminate the damping term in the equation of motion. Define the conformal time τ as

$$d\tau a(\tau) \equiv dt = d\eta/H. \tag{89}$$

In conformal time, the mode equation becomes

$$\partial_\tau^2 \Psi^{(j)} + W^2 \Psi^{(j)} = 0 \tag{90}$$

where

$$W^2 \equiv M^2(\tau) H^2 a^2 - \frac{\partial_\tau^2 a}{a} I \tag{91}$$

$$\Psi^{(j)} \equiv a \psi^{(j)}. \tag{92}$$

Because M^2contains $[k^2/(aH)^2]I$, the eigenvectors of W^2 are the same as those of M^2 with the replacement

$$k^2 \to \bar{k}^2 \equiv k^2 - \frac{\partial_\tau^2 a}{a} = k^2 - \left(\dot{a}^2(t) + a(t)\ddot{a}(t)\right) \tag{93}$$

and the eigenvalues of W^2 are

$$\omega_j^2(\tau) \equiv (Ha)^2 E_j^2(\tau) \quad \text{with the replacement } k^2 \to k^2 - 2a^2H^2 \text{ in } W_D^2. \tag{94}$$

The leading adiabatic order WKB solution is then

$$\Psi^{(j)(0)}(\tau) = \frac{1}{2} \frac{\mathscr{V}^{(j)}(\tau)}{\sqrt{\omega_j(\tau)}} \exp\left[-i \int_{\tau_i}^{\tau} d\tau'' \omega_j(\tau'')\right] \tag{95}$$

where

$$\mathscr{V}^{(j)}(\tau) = \mathscr{N}_j(\tau) \begin{pmatrix} a_j(\tau) \\ b_j(\tau) \\ c_j(\tau) \\ d_j(\tau) \end{pmatrix} \tag{96}$$

and the normalization is consistent with Eqs. (85) and (87). The solutions $\Psi^{(j)(0)}$ will no longer be a good approximation when

$$\left[\frac{1}{2}\frac{\partial_\tau^2 \omega_j}{\omega_j^3} - \frac{3}{4}\left(\frac{\partial_\tau \omega_j}{\omega_j^2}\right)^2\right] \mathscr{V}^{(j)} - \frac{\partial_\tau^2 \mathscr{V}^{(j)}}{\omega_j^2} + \frac{\partial_\tau \omega_j}{\omega_j^3} \partial_\tau \mathscr{V}^{(j)} + \frac{2i}{\omega_j} \partial_\tau \mathscr{V}^{(j)} \gg \mathscr{V}^{(j)} \tag{97}$$

for the nonzero elements of $\mathscr{V}^{(j)}$. Note that when $\tilde{\Phi}_+(t)/F_a \gg 1$, the WKB solution Eq. (95) will be a good approximation for heavy modes (i.e. modes $E_j(k=0) \gg 1$).

For small ω_j functions (*i.e.* $j = 1,3$), breakdown of $\Psi^{(j)(0)}$ approximation can occur due to terms such as $(\partial_\tau \omega_j/\omega_j^2)^2$ in Eq. (97) before the nonadiabaticity associated with $\partial_\tau^2 \mathscr{V}^{(j)}$ (i.e. turning points of the usual 1-dimensional WKB approximation). To separate these distinct nonadiabatic behaviors, we define a semi-numerical mode function $\Psi^{(j)}_{\text{trial}}(\tau) \equiv \mathscr{V}^{(j)}(\tau) f^{(j)}(\tau)$ where $f^{(j)}(\tau)$ satisfies the scalar mode equation

$$\partial_\tau^2 f^{(j)} + \omega_j^2(\tau) f^{(j)} = 0 \tag{98}$$

with adiabatic boundary conditions:

$$f^{(j)}(\tau_i) = \frac{1}{2\sqrt{\omega_j(\tau_i)}} \qquad \partial_\tau f^{(j)}(\tau_i) = -i\frac{1}{2}\sqrt{\omega_j(\tau_i)}. \tag{99}$$

(In practice, we solve this equation also in the variable $\eta \equiv Ht$ instead of in the conformal time τ.) Note that $\Psi^{(j)}_{\text{trial}}(\tau)$ satisfies the mode equations whenever $\partial_\tau^2 \mathscr{V}^{(j)}(\tau)$ and $\partial_\tau \mathscr{V}^{(j)}(\tau)$ vanishes. Hence, we can define a measure of how well $\Psi^{(j)}_{\text{trial}}$ satisfies the mode equation as

$$\mathscr{E}_{\text{na}(j)}(\tau) \equiv \frac{\left|\left[\partial_\tau^2 + W^2(\tau)\right] \Psi^{(j)}_{\text{trial}}\right|}{f^{(j)} \omega_{\text{eff}}^2} \tag{100}$$

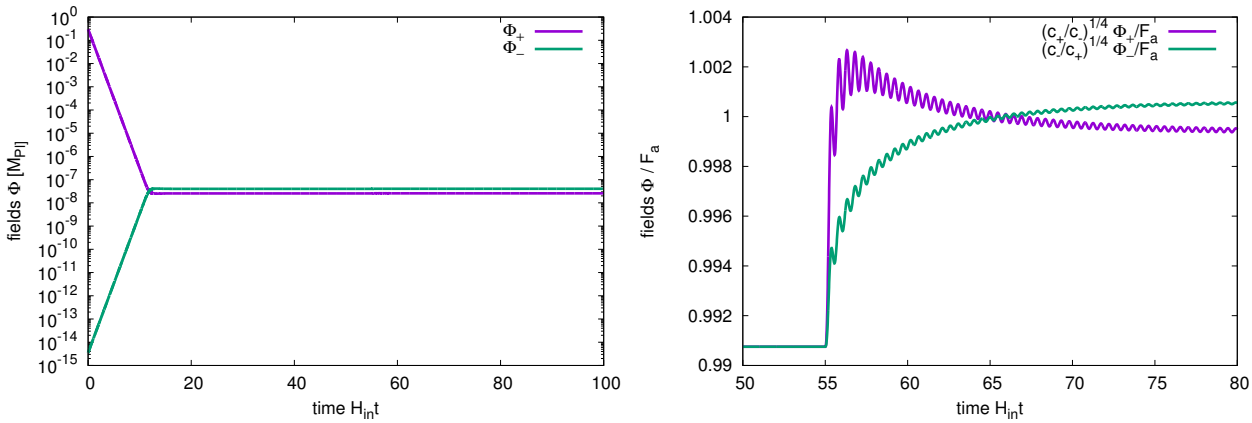

Figure 1: Homogeneous background field values for a model with $c_+ = 2.235$, $c_- = 0.9$, $\theta_+(t_i) = 0.04$, $h = 1$, $F_a = 7.9 \times 10^{10}$ GeV, $H = 9 \times 10^9$ GeV, and $\tilde{\Phi}_+(\eta_i) = 0.3\, M_{\rm Pl}$. (Left) The fields relax to $\sim F_a$ in ~ 10 e-folds. (Right) After inflation ends at $H_{\rm in} t = 55$, the fields undergo damped oscillation. On the horizontal axis of these plots, we have denoted $H_{\rm in}$ as the expansion rate at the initial time $t_i = 0$ to emphasize the fact that the plots actually continue to the time period after the end of inflation when the expansion rate starts to decrease. In the text where we primarily discuss the approximately constant expansion rate during inflation, we denote $H_{\rm in}$ simply as H.

where $\omega^2_{\rm eff}$ should be of order ω_j^2 to measure the validity of the approximation. Since the dominant contribution to $\mathscr{E}_{{\rm na}(j)}(\tau)$ should come from the the lightest ω_j which has effective mass terms of order $(c_+ - 2)a^2H^2$ and since we will be concerned with the j that maximizes $\mathscr{E}_{{\rm na}(j)}(\tau)$, we choose a positive definite quantity

$$\omega^2_{\rm eff} \equiv \sqrt{k^4 + (c_+ - 2)^2 (a^2H^2)^2} \tag{101}$$

independently of j. For a computation accurate to about 5%, we can define the time η_{NA} (in the variable $\eta = Ht$) satisfying

$$\max_j \mathscr{E}_{na(j)}(\tau(\eta_{NA})) = O(0.05) \tag{102}$$

after which one can no longer use $\Psi^{(j)}_{\rm trial}(\tau)$ for all j as an approximation. For $\eta > \eta_{NA}$, we numerically solve Eq. (40) with the boundary conditions

$$\psi(\eta_{NA}) = \mathscr{V}^{(j)}(\tau(\eta_{NA})) \left[\frac{f^{(j)}(\tau(\eta_{NA}))}{a(\tau(\eta_{NA}))} \right] \tag{103}$$

$$\psi'(\eta_{NA}) = \partial_\eta \left[\mathscr{V}^{(j)}(\tau(\eta)) \left[\frac{f^{(j)}(\tau(\eta))}{a(\tau(\eta))} \right] \right]_{\eta=\eta_{NA}} . \tag{104}$$

4. NUMERICAL CALCULATIONS

4.1. Homogeneous solution

Since the evolution of the background fields $\tilde{\Phi}_\pm$ is described by coupled non-linear equations of motion in which $\tilde{\Phi}_+$ and $\tilde{\Phi}_-$ initially differ by $2\log_{10}(M_{\rm Pl}/F_a) \approx 15$ orders of magnitude, we integrate the system numerically using the Class Library for Numbers (CLN) arbitrary-precision arithmetic package [31]. This is done using our own implementation of a 4th-order Runge-Kutta-Fehlberg ordinary differential equation solver with adaptive step size control, using 50 digits of precision and a numerical tolerance of 10^{-20}.

Figure 1 shows our results for a particular model. Clearly evident are three different regimes of field evolution: early inflation, late inflation, and post-inflation. During the early inflationary period, $\tilde{\Phi}_+\tilde{\Phi}_- \approx F_a^2$ to excellent precision as $\tilde{\Phi}_+$ rolls down its potential. In the approximation of neglecting inflationary slow-roll parameters, $\tilde{\Phi}''_+ + 3\tilde{\Phi}'_+ + c_+\tilde{\Phi}_+ = 0$, implying $\tilde{\Phi}_+(\eta) =$

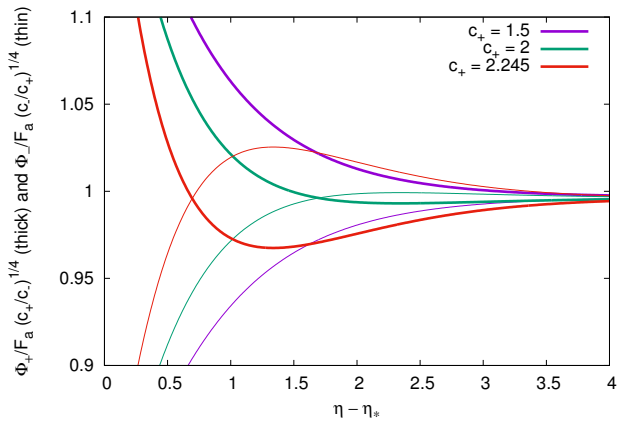

Figure 2: The transition from rolling to constant fields is not always monotonic. $\tilde{\Phi}_+$ (thick lines) and $\tilde{\Phi}_-$ (thin lines) overshoot their final values of Eq. (108) for sufficiently large c_+.

$\tilde{\Phi}_+(\eta_i)\exp(-\gamma\eta)$ for constant γ. Then $\tilde{\Phi}_+\tilde{\Phi}_- \approx F_a^2$ implies $\tilde{\Phi}_- \propto \exp(\gamma\eta)$. We may approximate $\tilde{\Phi}_-$ early during inflation by applying this ansatz to the $\tilde{\Phi}_-$ equation of motion, leading to the early-inflation approximations

$$\gamma = \frac{3}{2}\left(1-\sqrt{1-\frac{4}{9}c_+}\right) \tag{105}$$

$$\tilde{\Phi}_+(\eta) = \tilde{\Phi}_+(\eta_i)\exp(-\gamma\eta) \tag{106}$$

$$\tilde{\Phi}_-(\eta) = \frac{F_a^2\tilde{\Phi}_+}{\tilde{\Phi}_+^2+(\gamma^2+3\gamma+c_-)H^2/h^2}. \tag{107}$$

Once $\tilde{\Phi}_\pm \sim F_a$, the field values stabilize at the following potential minima:

$$\frac{\tilde{\Phi}_\pm}{F_a} = \left(\frac{c_\mp}{c_\pm}\right)^{1/4}\sqrt{1-\frac{\sqrt{c_+c_-}H^2}{h^2F_a^2}}. \tag{108}$$

In the small-H/F_a approximation, the time and wavenumber associated with the transition from early to late inflation can be found by setting the early-inflation $\tilde{\Phi}_+$ approximation equal to $F_a(c_-/c_+)^{1/4}$:

$$\eta_\star = \frac{1}{\gamma}\log\left[\frac{\tilde{\Phi}_+(\eta_i)}{F_a}\left(\frac{c_+}{c_-}\right)^{1/4}\right] \tag{109}$$

$$\frac{k_\star}{H} = \exp(\eta_\star) = \left(\frac{\tilde{\Phi}_+(\eta_i)}{F_a}\right)^{\frac{1}{\gamma}}\left(\frac{c_+}{c_-}\right)^{\frac{1}{4\gamma}} \tag{110}$$

where we have set $a(\eta=0)=1$. All k/H in this section can be interpreted as $k/[Ha(\eta=0)]$.

The transition between the two regimes is not always monotonic. Figure 2 shows that for large c_+, $\tilde{\Phi}_\pm$ overshoot their final values. We will see that an accurate computation of this overshoot is necessary for calculating the final power spectrum.

4.2. Inhomogeneous solution

Given the homogeneous solution for each parameter set, we integrate the equations for linearized perturbations in $\Phi_\pm$ to find the power spectrum. The set of equations and the procedure used is described in Sec. 3. The initial condition described in Eqs. (85) and (87) for each k mode is set at time $\eta_{i\mathrm{num}}(k)$ when

$$\mathscr{R} \equiv \frac{k}{a(\eta_{i\mathrm{num}}(k))H} = 10. \tag{111}$$

Our results are shown in Figure 3 for a model with a soft blue spectrum $n_\mathrm{I}=2.27$ and one with a hard blue spectrum $n_\mathrm{I}=3.76$. First, note that the sum of all four modes is dominated by the $j=1$ mode, which at early times is dominated by I_+, and at late

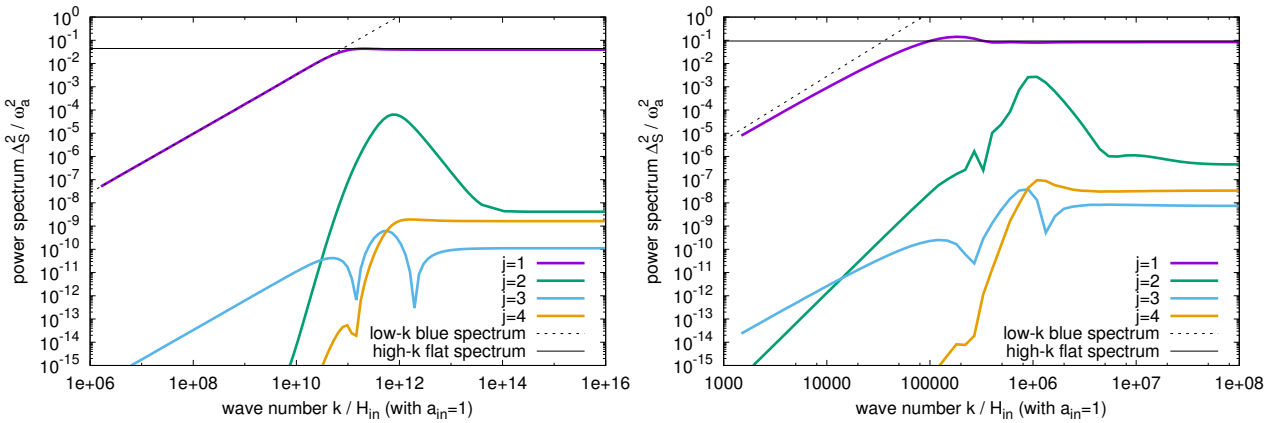

Figure 3: Power spectra $\Delta_S^2(k)/\omega_a^2$ for $c_+ = 1.5$ and $H = 6\times 10^9$ GeV (left) as well as $c_+ = 2.235$ and $H = 9\times 10^9$ GeV (right), corresponding to spectral indices of $n_{\rm I} = 2.27$ and $n_{\rm I} = 3.76$, respectively (shown as dotted lines). The other parameters, $h = 1$, $\theta_+(t_{\rm i}) = 0.04$, $c_- = 0.9$, and $F_{\rm a} = 7.9\times 10^{10}$ GeV are the same for both models. (See Fig. 1 for an explanation of $H_{\rm in}$.) These power spectra are evaluated at $H_{\rm in}t = 100$, long after the end of inflation.

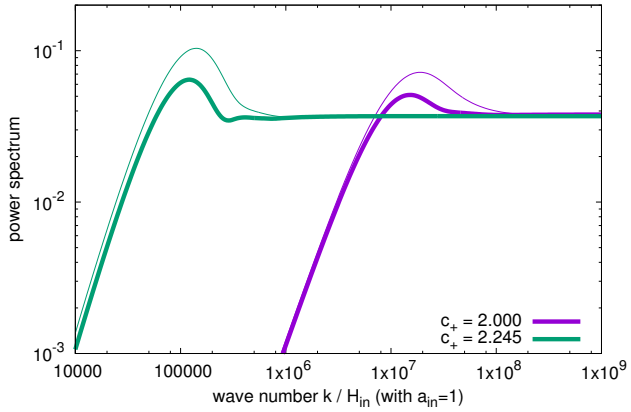

Figure 4: Peaks of $\Delta_S^2(k)/\omega_a^2$, calculated using the numerical solutions of Sec. 4.1 (thick lines) as well as a smoothed homogeneous solution interpolating Eqs. (106), (107), and (108) (thin lines). (See Fig. 1 for an explanation of $H_{\rm in}$.) These plots are evaluated at $H_{\rm in}t = 100$, long after the end of inflation.

times is a mixture of I_- and I_+. Since we are interested in approximating the power spectrum at the $\approx 10\%$ level, we can neglect all but the $j = 1$ mode henceforth.

Secondly, the hard blue power spectrum has a peak corresponding to the transition from blue to flat. Evidently, $\Delta_S^2(k)/\omega_a^2$ overshoots its large-k value and then falls back down, with a width of around an e-fold. This peak is a distinct feature that can facilitate the detection or exclusion of such models.

In order to investigate the dependence of this power spectrum peak on the transition from rolling to constant homogeneous fields $\Phi_\pm$, we constructed a smoothed approximation to the numerically-computed homogeneous fields of Sec. 4.1. We approximated $\tilde{\Phi}_+$ by adding Eqs. (106) and (108) in quadrature, and $\tilde{\Phi}_-$ by replacing γ by $-d\log(\tilde{\Phi}_+)/d\eta$ in Eq. (107). Figure 4 compares the power spectra resulting from the numerically-computed fields to their smoothed counterparts. Evidently the smoothing enhances the amplitude of the power spectrum feature by a factor of about two, even though the overshoot feature seen in Fig. 2 is only a $5\% - 10\%$ effect. Thus the accurate numerical computations of the homogeneous background fields in the nonadiabatic region are necessary even for $\approx 10\%$ accuracy in the final power spectrum.

Figure 5 shows that factor-of-two changes in h result in only small changes to the power spectrum. Decreasing or increasing h has the effect of shifting the power spectrum peak slightly to the left or the right, respectively. Since we have no compelling reason for choosing h an order of magnitude away from unity, and we are interested in a power spectrum calculation at the $\approx 10\%$ level, we do not study h further.

Finally, we investigate the evolution of the perturbations through the end of inflation. Figure 6 shows that they increase in magnitude by $\approx H^2/F_{\rm a}^2 \approx 1\%$ after the end of inflation, and undergo damped oscillations at the $\approx 0.1\%$ level, similar to

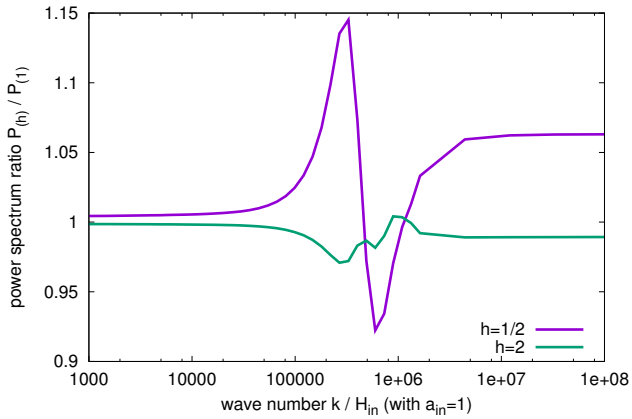

Figure 5: Fractional change in the power spectrum due to the variation of h from 1. The remaining parameters are identical to those used in Figure 3 (bottom). (See Fig. 1 for an explanation of $H_{\rm in}$.) These plots are evaluated at $H_{\rm in}t = 100$, long after the end of inflation.

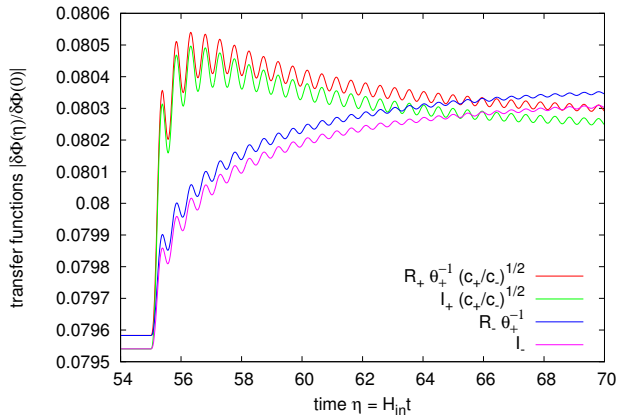

Figure 6: Field perturbations for a single mode after the end of inflation, $\eta = 55$, for the $c_+ = 2.235$ model shown in Fig. 1. (See Fig. 1 for an explanation of $H_{\rm in}$.)

the homogeneous fields $\Phi_\pm$ in Fig. 1. Thus the perturbations evolve adiabatically through the end of inflation, without any significant suppression or amplification due to oscillations in $\Phi_\pm$.

4.3. Fitting function

As we saw in the previous subsection, the power spectrum is sensitively dependent on the details of the homogeneous field evolution, which is computationally expensive to determine. Furthermore, we would like to constrain blue-tilted isocurvature models such as this one using large-scale structure data. A power spectrum needing several parameters to describe its broad features and several more for the peak feature would be poorly constrained by the data.

In this section we construct a fitting function describing the power spectrum in terms of 3 independent parameters: the blue tilt $n_{\rm I} = 2\gamma + 1$, determined by c_+; the transition scale $k_\star/H$, given in Eq. (110); and the overall amplitude, as we explain further below. We fit the other features of the power spectrum, including the amplitude and the width of the peak associated with the blue-to-flat transition, in terms of these three. The scaling of our parameters with c_- is also given. Since varying h by a factor of two is found to result in $< 10\%$ changes to the power spectrum, we fix $h = 1$ henceforth.

As a starting point, we choose a broken power law model characterized by a high-k amplitude A, a blue-to-flat ratio ρ, and a dimensionless width parameter w, as $A\left[1 + (\rho(k/k_\star)^{2\gamma})^{-1/w}\right]^{-w}$. Here w is of the order of the number of e-folds over which the transition from blue to flat takes place. Judging from Fig. 3, w is of order unity, and is larger for bluer tilts. In order to fit the power spectrum peak, we choose a Lorentzian function characterized by an amplitude α, a center μ, and a width σ, as well as a skew parameter λ characterizing the asymmetry of the peak. Our fitting function, valid in the $\theta_+(t_{\rm i}) \ll 1$ and $H/F_{\rm a} \ll 1$ limits,

c_+	$\tilde{A}$	$\tilde{\rho}$	w	α	μ	σ	λ
1.500	0.9036	1.123	0.3558	0.1333	0.4554	0.2894	0.01114
1.600	0.9015	1.145	0.3799	0.1743	0.3805	0.3393	0.01116
1.700	0.8989	1.168	0.425	0.2261	0.3131	0.3779	0.008246
1.800	0.896	1.188	0.4986	0.2942	0.2518	0.4052	0.004133
1.900	0.8924	1.204	0.6192	0.3918	0.192	0.4268	-0.003754
1.950	0.8904	1.208	0.7109	0.4614	0.1606	0.4398	-0.01367
2.000	0.8885	1.208	0.8426	0.5595	0.1264	0.4601	-0.03494
2.025	0.8876	1.205	0.9328	0.628	0.1078	0.4756	-0.05327
2.050	0.8873	1.198	1.054	0.723	0.08889	0.4994	-0.08532
2.075	0.8891	1.182	1.252	0.8889	0.07784	0.5481	-0.1664
2.100	0.8926	1.158	1.574	1.212	0.06334	0.6359	-0.2712
2.125	0.8968	1.125	1.965	1.717	0.02296	0.7236	-0.306
2.150	0.9019	1.086	2.338	2.304	-0.01774	0.777	-0.2973
2.175	0.9077	1.036	2.715	2.985	-0.05606	0.8078	-0.2734
2.200	0.9148	0.9593	3.173	3.934	-0.1002	0.8302	-0.2392
2.210	0.9185	0.9129	3.401	4.46	-0.1208	0.838	-0.2228
2.220	0.9229	0.8481	3.672	5.129	-0.1435	0.8452	-0.2049
2.230	0.9284	0.7483	4.017	6.063	-0.1699	0.8528	-0.1845
2.235	0.932	0.6735	4.236	6.699	-0.1852	0.8565	-0.173
2.240	0.9365	0.567	4.509	7.553	-0.2028	0.8604	-0.1599
2.245	0.9429	0.3962	4.895	8.877	-0.2254	0.8651	-0.1438
2.249	0.9525	0.1323	5.481	11.2	-0.2556	0.8709	-0.1237

Table I: Best-fitting parameters for the fitting function of Eqs. (112), (113), (114), and (115), with A and ρ expressed in terms of the rescaled amplitudes $\tilde{A} = A\mathscr{R}^3(1+c_-/c_+)/\sqrt{\mathscr{R}^2+c_+-2}$ and $\tilde{\rho} = 2\pi\rho/[2^{2\nu}\Gamma(\nu)^2(1+c_+/c_-)]$ with $\nu = \sqrt{9/4-c_+}$.

Model:	Small-c_+	Medium-c_+	High-c_+
c_+	0.1596	1.942	2.236
c_-	0.597	0.855	0.548
$\theta_+(t_\mathrm{i})$	0.0877	0.0272	0.0209
F_a [GeV]	9.30×10^{11}	3.44×10^{10}	1.46×10^{10}
H [GeV]	6.57×10^{10}	2.76×10^{9}	7.23×10^{8}
$\tilde{\Phi}_+(\eta_i)/M_\mathrm{Pl}$	0.226	0.452	0.117

Table II: Models with randomly-chosen parameters, used for testing the fitting function of Eqs. (112), (113), (114), and (115). In all cases, $h=1$ is fixed. The dark matter fractions ω_a corresponding to these parametric choices are 0.027 (small-c_+), 5×10^{-5} (medium-c_+), and 10^{-5} (high-c_+).

takes the form

$$\frac{\Delta^2_\mathrm{fit}(k)}{\omega^2_\mathrm{a}} = \frac{\mathscr{R}^3 H^2\sqrt{c_-/c_+}}{4\pi^2 F_\mathrm{a}^2\theta_+(t_\mathrm{i})^2\sqrt{\mathscr{R}^2+c_+-2}}\left|T_{I_-}\right|^2 \tag{112}$$

$$\left|T_{I_-}\right|^2 = A\frac{1+\alpha L\left(\frac{\ln(k/k_\star)-\mu}{\sigma}\right)S\left(\lambda\,\frac{\ln(k/k_\star)-\mu}{\sigma}\right)}{\left[1+(\rho(k/k_\star)^{2\gamma})^{-1/w}\right]^w} \tag{113}$$

$$L(x) = 1/(1+x^2) \tag{114}$$

$$S(x) = 1+\tanh(x). \tag{115}$$

The seven parameters in $\left|T_{I_-}\right|^2$ are determined by minimizing the mean-squared difference between $\Delta^2_\mathrm{fit}(k)$ and numerical computations over 100 logarithmically-spaced bins in the range $10^{-3}k_\star \le k \le 10^3 k_\star$. Table I shows our results for a range of c_+ values from 1.5 to 2.249, corresponding to $2.27 \le n_\mathrm{I} \le 3.94$. Note that $n_\mathrm{I} \gtrsim 2.4$ is phenomenologically significant because such blue isocurvature spectral indices require a time dependent mass transition [15] for the isocurvature field degree of freedom just as in the particular axion model being studied here. Table I can be used for computing the isocurvature spectrum for a continuous family of model parameters by interpolating the seven parameters A, ρ, w, α, μ, σ, and λ from the table, finding $\left|T_{I_-}\right|^2$ using Eqs. (113), (114), and (115), and then substituting this into Eq. (112).

Finally, we test our fitting function for three models randomly chosen to have small ($1.5 < c_+ < 1.7$), medium ($1.9 < c_+ < 2.1$), and large ($2.235 < c_+ < 2.245$) values of c_+. The other parameter have been chosen using uniform random distributions with $0.5 < c_- < 1$, $0.01 < \theta_+(t_\mathrm{i}) < 0.1$, $10 < \log_{10} F_\mathrm{a}[\mathrm{GeV}] < 12$, $0.01 < H/F_\mathrm{a} < 0.1$, and $0.1 < \tilde{\Phi}_+(\eta_i)/M_\mathrm{Pl} < 1$. The models chosen are listed in Table II. Figure 7 shows the numerically computed power spectra along with our fitting functions. In each case, the power spectra have been divided by a "no-wiggle" power spectrum defined by setting $\alpha = 0$ in the corresponding fitting function. The figure shows that the fitting function of Eqs. (112), (113), (114), and (115) is accurate at the $10\% - 20\%$ level for

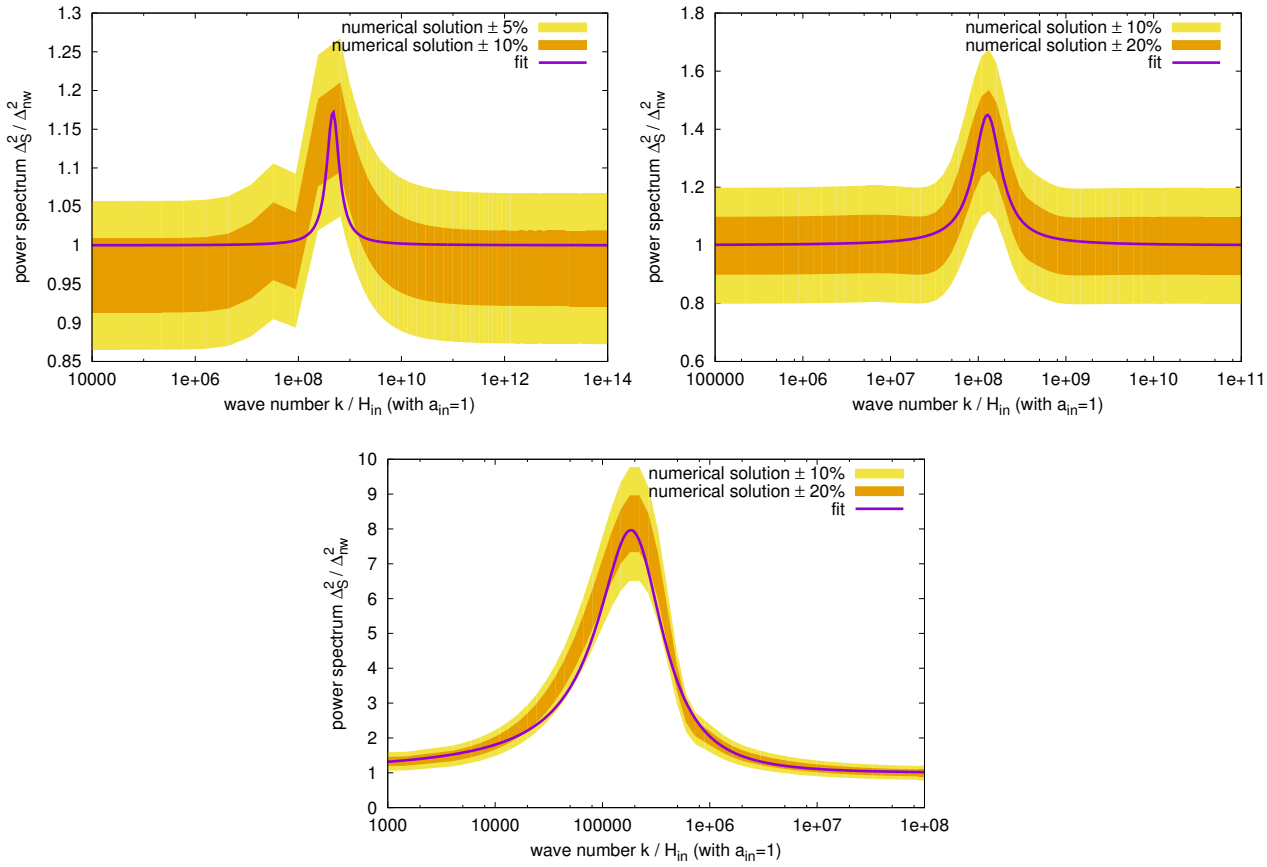

Figure 7: Tests of our fitting function for randomly-chosen model parameters, as given in Table II. For clarity, power spectra have been divided by "no-wiggle" spectra $\Delta^2_{\rm nw}$ found by setting $\alpha = 0$ in the fitting function. (Top-left) Small-c_+. (Top-right) Medium-c_+. (Bottom) High-c_+.

a wide range of models.

Instead of dealing with the axion model parameters directly, it may be a bit clearer for phenomenology to explicitly choose 3 parameters for the fits. Note that our fitting function Eq. (112) is of the form

$$F^2_{\rm fit\,gen}(k,k_\star,n_I,\mathscr{Q}_1,\mathscr{Q}_2) = \mathscr{Q}_1 \frac{1+\alpha(n_I)L\left[\frac{1}{\sigma(n_I)}\ln\left(e^{-\mu(n_I)}\frac{k}{k_\star}\right)\right]S\left[\frac{\lambda(n_I)}{\sigma(n_I)}\ln\left(e^{-\mu(n_I)}\frac{k}{k_\star}\right)\right]}{\left[1+\left(\mathscr{Q}_2\left(\frac{k}{k_\star}\right)^{n_I-1}\right)^{-1/w}\right]^w} \tag{116}$$

where one can make parameters such as α functions of a generic spectral index parameter n_I through the Table I using the map

$$c_+(n_I) = \frac{1}{4}(n_I-1)(7-n_I). \tag{117}$$

This is naively a function of 4 parameters: $\mathscr{Q}_{1,2}$, k_*, and n_I. However, within the limited range of c_- considered here, $\mathscr{Q}_2$ is independent of c_- at the level of accuracy we were aiming for. This means $\mathscr{Q}_2$ can be extracted from $\tilde{\rho}$ in Table I after fixing $c_- = 0.9$ used in making the table: *i.e.*

$$\mathscr{Q}_2 = \rho(n_I) = \tilde{\rho}(n_I)2^{2\sqrt{\frac{9}{4}-c_+(n_I)}}\frac{\Gamma^2\left(\sqrt{\frac{9}{4}-c_+(n_I)}\right)}{2\pi}\left(1+\frac{c_+(n_I)}{0.9}\right). \tag{118}$$

Hence in hunting for this lamp post model signatures in future data, we advocate using

$$\boxed{\Delta^2_S(k;k_\star,n_I,\mathscr{Q}_1) = F^2_{\rm fit\,gen}\left(\frac{k}{k_\star},n_I,\mathscr{Q}_1,\rho(n_I)\right)} \tag{119}$$

which is explicitly a function of 3 parameters $k_\star$, n_I, and $\mathscr{Q}_1$. It is interesting that even though one would generically expect that there are at least 5 parameters describing a break spectrum with a bump (*e.g.* overall amplitude, break location, flat spectrum amplitude, bump height, and bump width), the underlying axion model has approximately reduced this to only 3 independent parameters. After doing such a fit, the interpretation of best fit $\mathscr{Q}_1$ in the context of our axion model would be

$$\mathscr{Q}_1 = \left(\frac{H}{2\pi}\right)^2 \frac{\tilde{A}(c_+)\sqrt{c_-/c_+}}{F_{\rm a}^2\theta_+(t_{\rm i})^2(1+c_-/c_+)}\omega_{\rm a}^2 \tag{120}$$

where ω_a is the dark matter fraction in axions defined in Eq. (32) and is approximately

$$\omega_{\rm a} \approx W_a\theta_+(t_{\rm i})^2 \left(\frac{\sqrt{2}F_a\sqrt{\frac{c_-+c_+}{\sqrt{c_-c_+}}}}{10^{12}{\rm GeV}}\right)^{n_{PT}} \tag{121}$$

where we have assumed that $c_\pm > 0$.

Despite there being an upper limit on the spectral break location $k_\star$ within this axion model coming from the the fact $\tilde{\Phi}_+(\eta_i)$ is sub-Planckian at initial times, it is not extremely constraining. For example, setting $\tilde{\Phi}_+(\eta_i) \lesssim M_p$ at initial times, the constraint on $k_\star$ is

$$\frac{k_\star}{H} \lesssim \left(\frac{M_p}{F_{\rm a}}\right)^{\frac{2}{n_I-1}} \left(\frac{c_+}{c_-}\right)^{\frac{1}{2(n_I-1)}}. \tag{122}$$

If F_a is expressed in terms of dark matter fraction ω_a with $c_+ = c_- = 1$ and $n_I = 3.94$, this bound becomes

$$\frac{k_\star}{H} \lesssim 10^5 \left(\frac{\theta_+(t_{\rm i})}{4\times 10^{-2}}\right)^{1.14} \left(\frac{\omega_a(\theta_+(t_{\rm i})\text{ fixed})}{10^{-5}}\right)^{-0.57}. \tag{123}$$

The left hand side of this inequality can be interpreted in terms of length scales today as

$$\frac{k_\star}{a(\text{today})} \approx 1\,{\rm Mpc}^{-1} e^{-(N_e-54)} \left(\frac{k_\star/H}{10^5}\right)\left(\frac{T_{\rm rh}}{10^7{\rm GeV}}\right)^{1/3}\left(\frac{H}{7\times 10^8{\rm GeV}}\right)^{1/3}\left(\frac{g_{*S}(t_0)}{3.9}\right)^{1/3} \tag{124}$$

where N_e is the number of e-folds between t_i and the end of inflation, $T_{\rm rh}$ is the reheating temperature, $g_{*S}(t_0)$ is the effective number of entropy degrees of freedom today.[7] Since the scales accessible to cosmological experiments are approximately

$$10^{-3}\,{\rm Mpc}^{-1} \lesssim k/a(\text{today}) \lesssim {\rm Mpc}^{-1}, \tag{125}$$

we see from Eqs. (123) and (124) that it is not difficult to arrange the break in a region that is observable by changing the inflationary/reheating model (*e.g.* decrease $T_{\rm rh}$ and/or increase the number of e-folds), increasing the dark matter fraction ω_a, and/or decrease the initial condition field value of $\tilde{\Phi}_+(\eta_i)$. It is also not difficult to push $k_\star$ outside of the observable region by increasing $\theta_+(t_{\rm i})$ even with the inflationary/reheating model fixed to the canonical values shown in Eq. (124). The extraction of $\mathscr{Q}_1$ will contain information about $H/F_{\rm a}$ that can be varied independently of ω_a. Its implication for the tensor-to-scalar ratio was already explored in [28]. Perturbativity and/or the linear fluctuation approximation must be reanalyzed for $k \gtrsim k_\star$ modes when $H/(2\pi\theta_+(t_{\rm i})F_{\rm a})$ implied by the best fit parameters is larger than unity. Finally, as noted above, the spectral index $n_I \leq 3.94$ bound should be enforced when fitting since only that range has been tabulated Table I.

Given the general field theory model degeneracies that exist if one fixes only the two-point function, Eq. (119) is likely to be more general than the specific underlying model used to inspire it. The utility of this paper is to show that this parameterization is consistent with at least one realistic underlying field theory model.

5. CONCLUSIONS

In observable blue isocurvature spectral models, there is a break in the spectrum corresponding to the mass of the isocurvature field undergoing a transition [15, 24]. Analytic techniques typically break down in this spectral regime [28] because of a

[7] The main approximation in this formula is the neglect of the slow-roll evolution of the expansion rate H during inflation. We have also assumed that there is exactly one inflationary period and its attendant reheating since the time t_i.

combination of nonadiabatic time-dependence of the mass matrix and the non-linearity of the time dependent background field equations which govern the mass matrix. We have computed the isocurvature perturbations and the observable spectrum for the axion model of [24] numerically in this region. We find a bump near the break in the spectrum that enhances the blue isocurvature signal by almost a factor of two for a steep spectral index. We constructed an economical 3-parameter fitting function Eq. (119) which reproduces the bump at the 20% accuracy level. Although this fitting function has been checked only against the particular axion model studied in this paper, the qualitative form of the bump connecting two spectral regions may be generic. Hence, this "lamp-post" model computation is likely to be useful for future hunt for blue isocurvature contributions to the cosmic microwave background and large scale structure power spectra.

Acknowledgments

This work was supported in part by the DOE through grant DE-FG02-95ER40896.

---

[1] E. J. Copeland, A. R. Liddle, D. H. Lyth, E. D. Stewart and D. Wands, *False vacuum inflation with Einstein gravity*, *Phys. Rev.* **D49** (1994) 6410–6433, [astro-ph/9401011]. 1
[2] M. Dine, W. Fischler and D. Nemeschansky, *Solution of the Entropy Crisis of Supersymmetric Theories*, *Phys. Lett.* **B136** (1984) 169–174. 1
[3] O. Bertolami and G. G. Ross, *Inflation as a Cure for the Cosmological Problems of Superstring Models With Intermediate Scale Breaking*, *Phys. Lett.* **B183** (1987) 163–168.
[4] M. Dine, L. Randall and S. D. Thomas, *Supersymmetry breaking in the early universe*, *Phys.Rev.Lett.* **75** (1995) 398–401, [hep-ph/9503303]. 1
[5] A. D. Linde and V. F. Mukhanov, *Nongaussian isocurvature perturbations from inflation*, *Phys. Rev.* **D56** (1997) 535–539, [astro-ph/9610219]. 1
[6] S. Weinberg, *Must cosmological perturbations remain non-adiabatic after multi-field inflation?*, *Phys. Rev.* **D70** (2004) 083522, [astro-ph/0405397]. 1
[7] Y. Takeuchi and S. Chongchitnan, *Constraining isocurvature perturbations with the 21cm emission from minihaloes*, 1311.2585. 1
[8] J. B. Dent, D. A. Easson and H. Tashiro, *Cosmological constraints from CMB distortion*, *Phys.Rev.* **D86** (2012) 023514, [1202.6066].
[9] J. Chluba and D. Grin, *CMB spectral distortions from small-scale isocurvature fluctuations*, *Mon.Not.Roy.Astron.Soc.* **434** (2013) 1619–1635, [1304.4596].
[10] T. Sekiguchi, H. Tashiro, J. Silk and N. Sugiyama, *Cosmological signatures of tilted isocurvature perturbations: reionization and 21cm fluctuations*, *JCAP* **1403** (2014) 001, [1311.3294]. 1
[11] X. Chen and Y. Wang, *Quasi-Single Field Inflation and Non-Gaussianities*, *JCAP* **1004** (2010) 027, [0911.3380]. 1
[12] N. Craig and D. Green, *Testing Split Supersymmetry with Inflation*, *JHEP* **07** (2014) 102, [1403.7193].
[13] N. Arkani-Hamed and J. Maldacena, *Cosmological Collider Physics*, 1503.08043.
[14] E. Dimastrogiovanni, M. Fasiello and M. Kamionkowski, *Imprints of Massive Primordial Fields on Large-Scale Structure*, *JCAP* **1602** (2016) 017, [1504.05993]. 1
[15] D. J. H. Chung, *Large blue isocurvature spectral index signals time-dependent mass*, *Phys. Rev.* **D94** (2016) 043524, [1509.05850]. 1, 4.3, 5
[16] R. Peccei and H. R. Quinn, *CP Conservation in the Presence of Instantons*, *Phys.Rev.Lett.* **38** (1977) 1440–1443. 1
[17] S. Weinberg, *A New Light Boson?*, *Phys.Rev.Lett.* **40** (1978) 223–226.
[18] F. Wilczek, *Problem of Strong p and t Invariance in the Presence of Instantons*, *Phys.Rev.Lett.* **40** (1978) 279–282.
[19] J. E. Kim, *Weak Interaction Singlet and Strong CP Invariance*, *Phys. Rev. Lett.* **43** (1979) 103.
[20] M. A. Shifman, A. I. Vainshtein and V. I. Zakharov, *Can Confinement Ensure Natural CP Invariance of Strong Interactions?*, *Nucl. Phys.* **B166** (1980) 493–506.
[21] A. R. Zhitnitsky, *On Possible Suppression of the Axion Hadron Interactions. (In Russian)*, *Sov. J. Nucl. Phys.* **31** (1980) 260.
[22] M. Dine, W. Fischler and M. Srednicki, *A Simple Solution to the Strong CP Problem with a Harmless Axion*, *Phys. Lett.* **B104** (1981) 199–202.
[23] J. E. Kim and G. Carosi, *Axions and the Strong CP Problem*, *Rev. Mod. Phys.* **82** (2010) 557–602, [0807.3125]. 1
[24] S. Kasuya and M. Kawasaki, *Axion isocurvature fluctuations with extremely blue spectrum*, *Phys.Rev.* **D80** (2009) 023516, [0904.3800]. 1, 2, 5
[25] G. G. Raffelt, *Astrophysical axion bounds*, *Lect. Notes Phys.* **741** (2008) 51–71, [hep-ph/0611350]. 1
[26] P. Sikivie, *Axion Cosmology*, *Lect.Notes Phys.* **741** (2008) 19–50, [astro-ph/0610440].
[27] P. W. Graham, I. G. Irastorza, S. K. Lamoreaux, A. Lindner and K. A. van Bibber, *Experimental Searches for the Axion and Axion-Like Particles*, *Ann. Rev. Nucl. Part. Sci.* **65** (2015) 485–514, [1602.00039]. 1
[28] D. J. H. Chung and H. Yoo, *Elementary Theorems Regarding Blue Isocurvature Perturbations*, *Phys. Rev.* **D91** (2015) 083530, [1501.05618]. 1, 3, 4.3, 5
[29] M. Kawasaki and K. Nakayama, *Axions: Theory and Cosmological Role*, *Ann.Rev.Nucl.Part.Sci.* **63** (2013) 69–95, [1301.1123]. 3, 3

[30] X. Chen, M. H. Namjoo and Y. Wang, *On the equation-of-motion versus in-in approach in cosmological perturbation theory*, *JCAP* **1601** (2016) 022, [1505.03955]. 3.1

[31] "Class library for numbers." http://www.ginac.de/CLN/. 4.1